Translational Oncology 14 (2021) 101091

Contents lists available at ScienceDirect

Translational Oncology

journal homepage: www.elsevier.com/locate/tranon

A recombinant Chinese measles virus vaccine strain rMV-Hu191 inhibits human colorectal cancer growth through inducing autophagy and apoptosis regulating by PI3K/AKT pathway

Chu-di Zhang[a,b], Yi-long Wang[a], Dong-ming Zhou[a], Meng-ying Zhu[a,b], Yao Lv[a], Xiao-qiang Hao[a], Chu-fan Qu[a,b], Yi Chen[a,b], Wei-zhong Gu[a], Ben-qing Wu[c], Pei-chun Chen[c], Zheng-yan Zhao[a,b,*]

[a] Children's Hospital, Zhejiang University School of Medicine, Hangzhou 310052, Zhejiang. China
[b] Zhejiang University School of Medicine, Hangzhou 310000, Zhejiang. China
[c] University of Chinese Academy of Sciences Shenzhen Hospital, Shenzhen 518000, China

ARTICLE INFO

Keywords:
Colorectal cancer
Oncolytic measles virotherapy
Apoptosis
Autophagy
PI3K/AKT signaling pathway

ABSTRACT

The potential therapeutic effects of oncolytic measles virotherapy have been verified against plenty of malignancies. However, the oncolytic effects and underlying mechanisms of the recombinant Chinese measles virus vaccine strain Hu191 (rMV-Hu191) against human colorectal cancer (CRC) remain elusive. In this study, the antitumor effects of rMV-Hu191 were evaluated in CRC both *in vitro* and *in vivo*. From our data, rMV-Hu191 induced remarkably caspase-dependent apoptosis and complete autophagy *in vitro*. In mice bearing CRC xenografts, tumor volume was remarkably suppressed and median survival was prolonged significantly with intratumoral treatment of rMV-Hu191. To gain further insight into the relationship of rMV-Hu191-induced apoptosis and autophagy, we utilized Rapa and shATG7 to regulate autophagy. Our data suggested that autophagy was served as a protective role in rMV-Hu191-induced apoptosis in CRC. PI3K/AKT signaling pathway as one of the common upstream pathways of apoptosis and autophagy was activated in CRC after treatment with rMV-Hu191. And inhibition of PI3K/AKT pathway using LY294002 was accompanied by enhanced apoptosis and decreased autophagy which suggested that PI3K/AKT pathway promoted rMV-Hu191-induced autophagy and inhibited rMV-Hu191-induced apoptosis. This is the first study to demonstrate that rMV-Hu191 could be used as a potentially effective therapeutic agent in CRC treatment. As part of the underlying cellular mechanisms, apoptosis and autophagy were involved in the oncolytic effects generated by rMV-Hu191. And the cross-talk between these two processes and the PI3K/AKT signaling pathway was well identified.

1. Introduction

Colorectal cancer (CRC), a highly malignant tumor of the digestive system, is the fourth lethal malignancies worldwide due to its high mortality [1,2]. With the applications of conventional therapies such as surgery, adjuvant chemotherapy and radiotherapy, colorectal cancer could recur frequently after the initial treatment or even entire removal of the tumor. It is reported that the mean survival time of the CRC is still less than 3 years [3]. Thus, effective and promising therapeutic strategies are still urgently needed across the globe.

Oncolytic viruses (OVs) [4–6] which can selectively replicate in tumor cells and destroy them while leaving normal cells with little or no damage, have been studied in a variety of human carcinomas [7,8]. OVs lead to cell lysis and death mainly by generating specific cytotoxic effects between adjacent cells [9]. Targeted therapies of OVs have been a hot spot region in the medical community in past decades. The results emerging from clinical trials have certified the security and feasibility of oncolytic virotherapy and provided early indications of efficacy. H101 (a genetically engineered adenovirus) was first approved by CFDA in China as an oncolytic virus for head and neck tumors treatment in 2005. Then, in 2015, T-VEC (a genetically modified herpes simplex virus) was officially approved by FDA in America for melanoma therapy. Moreover, Phase I/II clinical trials using measles virus Edmonston strain are currently underway [10].

Measles virus (MV) is a single-strand RNA virus belonging to the Morbillivirus genus of the *Paramyxoviridae* family [11]. MV principally

* Corresponding author.
E-mail addresses: 21718442@zju.edu.cn (C.-d. Zhang), 11418155@zju.edu.cn (Y.-l. Wang), 21318243@zju.edu.cn (D.-m. Zhou), 11618182@zju.edu.cn (M.-y. Zhu), 21418068@zju.edu.cn (Y. Lv), 11718196@zju.edu.cn (X.-q. Hao), 21818469@zju.edu.cn (C.-f. Qu), 21918473@zju.edu.cn (Y. Chen), 6195013@zju.edu.cn (W.-z. Gu), wubenqing783@126.com (B.-q. Wu), 674870541@qq.com (P.-c. Chen), zhaozy@zju.edu.cn (Z.-y. Zhao).

https://doi.org/10.1016/j.tranon.2021.101091
Received 15 January 2021; Received in revised form 15 March 2021; Accepted 30 March 2021

employed three cellular receptors, covering CD46, Nectin-4 and SLAM, for targeting cell entrance [12–14]. Nectin-4 is highly expressed in epithelial cells and adenocarcinoma cells. Wild-type MV infects more efficaciously via the receptor SLAM, a membrane glycoprotein expressed mainly in immune cells. While most MV vaccine strains and laboratory engineered strains infect human cells predominantly through CD46, a cellular receptor ubiquitously expressed in all nucleated cells, more to point, with higher abundance in human tumor cells than normal cells. Due to the genome stability and long history of vaccination application in China, the rMV-Hu191 modified by our laboratory using the virus reverse genetic system with enhanced safety and immunogenicity has been considered remarkably appropriated for further research as a novel oncolytic agent [15–17]. Meanwhile, the effective oncolytic property of rMV-Hu191 on gastric cancer has been confirmed [18]. However, the mechanisms of the oncolytic effects of rMV-Hu191 on colorectal cancer remain unknown.

Apoptosis is a cascade amplifying reactions regulated by CASPs/caspases, a cysteine family of proteases [19]. It is consisted of intrinsic pathway triggering mitochondrial outer membrane permeabilization by activating caspase-9 and extrinsic pathway through a death receptor-mediated manner by activating caspase-8 both resulting the cleavage of caspase-3 and PARP. Apoptosis is intensively appreciated as a mechanism of regulating cell death to cytoplasm shrinkage and nuclear fragmentation while undergoing death stimulus or normal development and morphogenesis.

Autophagy is a process that relies on the lysosomal pathway by forming a double-layer membrane structure to remove degenerated or misfolded proteins as well as aging or damaged organelles under the administration of autophagy related genes (ATG), which is conducive to the maintenance of intracellular homeostasis [20]. Stimulated by multiple stress conditions, such as nutrients, hypoxia, low energy and organelle damage, autophagy is identified as a form of endogenous defense against inflammation, autoimmunity, and cellular differentiation disorders [21]. Under certain circumstances, autophagy can participate in cell survival or cell death process [22,23]. Failure of autophagy regulation will result in cell abnormality or even death.

Due to the dual characters of autophagy, the complex relationship between autophagy and apoptosis usually occurring simultaneously in cancers to coordinate cell survival and death, alters under certain circumstances, such as the exposed cellular environment and the involved stress levels. PI3K/AKT signaling pathway as one of the common upstream signals of apoptosis and autophagy, involved in cell growth, proliferation, migration and apoptosis, is usually dysregulated in multiple human cancers contributing to cancer pathogenesis and therapy resistance [24,25]. Accumulated evidences have proved the connection between colorectal tumorigenesis and PI3K/AKT pathway, however, the potential mechanism still needs further improvement [26,27].

In this research, we elaborated for the first time that rMV-Hu191 generated effectively oncolytic effects in human CRC both *in vitro* and *in vivo*. We investigated the role of autophagy in rMV-Hu191-induced apoptosis. Furthermore, the potential involvement of PI3K/AKT signaling pathway in rMV-Hu191-induced autophagy and apoptosis was investigated. Based on these available results, we expected to provide promising therapeutic strategies for human CRC.

2. Materials and methods

2.1. Cell lines and reagents

African green monkey kidney Vero cells were acquired from the American Type Culture Collection (ATCC, USA) and cultured in DMEM medium. Human CRC cells and human umbilical vein endothelial cells (HUVEC) were purchased from the Cell Bank of the Chinese Academy of Sciences, Shanghai, China. HT-29 and HCT-116 cells were cultured in McCoy's 5A medium, LS-174T cells were cultured in DMEM medium, SW620 cells were cultured in Leibovitz's medium, DLD-1 and HUVEC cells were cultured in RPMI 1640 medium. All medium (Life Technologies, USA) were supplemented with 10% FBS. Cells were cultured at 37 ˚C, 5% CO2 incubator.

Reagents: Z-VAD-FMK (ApexBio, A1902), Rapa (Sirolimus, MB1197), CQ (Sigma, C6628-25), LysoTracker Red (Beyotime, C1046) and LY294002 (ApexBio, A8250) were used at the final concentrations of 100 μM, 3 μM, 20 μM, 50 nM and 25 μM, respectively. For flow cytometry: human CD46-FITC-conjugated antibody (R&D Systems, FAB2005G, 1:100), human Nectin-4-PE-conjugated antibody (R&D Systems, FAB2659P, 1:100), Annexin V FITC Apoptosis Detection Kit (BD Biosciences, 556547). For Western blot analysis: anti-LC3B (Sigma, L7543, 1:1000), anti-p62 (abcam, ab109012, 1:1000), anti-β-actin (CST, 4970S, 1:5000), anti-gapdh (CST, 5174S, 1:5000), anti-caspase-3 (CST, 9665S, 1:1000), anti-PARP (CST, 9542S, 1:1000), anti-PTEN (abcam, ab32199, 1:1000), anti-total AKT (CST, 4691, 1:1000), anti-phospho-AKT^{Ser473} (CST, 4060, 1:1000), secondary HRP-linked anti-rabbit IgG (CST, 7074S, 1:3000), secondary HRP-linked anti-mouse IgG (CST, 7076S, 1:3000).

2.2. Virus construction and infection assays

The construction of rMV-Hu191-H-EGFP was obtained by inserting exogenous EGFP gene fragment in rMV-Hu191 as previously described [15]. The virus titers were determined on Vero cells by plaque forming unit assays (PFU). Cells were washed with PBS once, and then incubated with rMV-Hu191-H-EGFP at multiple MOIs for 1.5 h at 37 ˚C. Unabsorbed virus supernatant was exchanged with fresh medium.

2.3. Assessment of cytotoxicity in vitro

2×10^5-1×10^6 cells/well of CRC cells seeded in 6-well plates were infected with rMV-Hu191-H-EGFP at multiple MOIs. After 72 h post treatment, the medium was abolished and the plates were fixed with 4% paraformaldehyde in 4 ˚C refrigerator overnight. The next day, the remaining cells were stained with 0.1% crystal violet. And then rinsed twice gently with running water, air-dried and photographed under light microscope (Zeiss, Germany) with companion software.

2.4. Cell proliferation assays

After infection of LS-174T (5×10^3/well) and HT-29 (3×10^3/well) seeded in 96-well plates with multiple MOIs of rMV-Hu191-H-EGFP, cell proliferation was quantified four days by Cell Counting Kit-8 (DOJINDO, CK04). At indicated time, cells were cultured with 100 μL working solution consisted of 90 μL DMEM medium and 10 μL reagent, for 30 min at 37 ˚C and then recorded the absorbance at 450 nm using multifunctional microporous plate detector (PowerPacTM Basic, BIO-RAD).

2.5. Measurement of virus growth curve

LS-174T (1×10^6 cells/well) and HT-29 (7×10^5 cells/well) seeded into 6-well plates were treated with rMV-Hu191-H-EGFP at MOI of 0.1 and 1. Unabsorbed virus was abolished after 1.5 h and replaced with 2 mL fresh medium. The cells were scraped into medium at every 24 h interval, freeze-thawed twice, and centrifuged. The titers of progeny virus were then measured on Vero cells by TCID50 assays.

2.6. Flow cytometry

A total number of 1×10^6 cells harvested by trypsin without EDTA were blocked for 30 min in 2% BSA on ice avoiding light. For extracellular staining, CRC cells were incubated with human CD46-FITC or human Nectin-4-PE-conjugated antibody in PBS for one hour. And then washed with cold PBS before analysis.

As for the detection of apoptosis kit, the cells after above treatments were harvested, and resuspended into 1x binding buffer, with the cell

density of 1×10^6 cells /mL, stained with 5 μL Annexin V-fluorescein isothiocyanate (FITC) and 5 μL propidium iodide (PI) for 15 min avoiding light, and then detected by flow cytometry (Beckman Coulter, USA) within one hour. All data were analyzed by the Flowjo vX.0.7 software (Tree Star Inc, USA).

2.7. Construction of cell lines by lentivirus system

The plenti-LC3B-EGFP plasmid, a generous gift from Professor Xi Chen (Children's Hospital, Zhejiang University School of Medicine, China), and the shATG7 plasmid, purchased from Genechem (Shanghai, China), were packaged as lentivirus according to the GenePharma Recombinant Lentivirus Operation Manual and then transfected the CRC cells. After screening with puromycin, the single cell clone was screened by dilution to 96-well plates. Subsequently, CRC cells stably expressing LC3B-EGFP or knocked down of ATG7 were obtained by amplification.

2.8. Confocal microscopy

The CRC cells transfected with LC3B-EGFP plasmid were seeded in laser confocal petri dishes at a density of 1.5×10^5 per well and were infected with rMV-Hu191 (MOI = 0.5) and Rapa (an autophagy promotor, 3 μM) for 48 h. For labelling acidic compartments, 50 nM LysoTracker Red was added into the medium to incubate for 30 min. Then the working fluid was removed with fresh medium. Colocalizations of autophagosomes (LC3B-EGFP) and lysosomes (LysoTracker Red) were examined by confocal microscope (Zeiss, cLSM780) and companion software.

2.9. Transmission electron microscopy

1×10^6 cells treated as indicated experiments were harvested, fixed with 2.5% glutaraldehyde at 4 °C overnight, followed by 1% osmic acid fixation, 2% uranium acetate staining, rinsing, gradient dehydration, embedding and polymerization. Ultrathin sections were stained with uranyl acetate and lead citrate, and then imaged at an accelerated voltage of 100 KV using the Zeiss EM 10 transmission electron microscope (Berlin, Germany).

2.10. Western blot analysis

Cells collected at designed time were lysed in RIPA buffer containing protease inhibitor PMSF (Beyotime, ST506-2) and phosphatase inhibitor cocktail (Beyotime, P1081). Supernatant was harvested and centrifuged. The protein concentration was quantified using a BCA Protein Assay (Beyotime, P0010). 50 μg proteins per well were separated by SDS-PAGE gels, and then transferred onto PVDF membranes (BIO-RAD, 1620177). The PVDF membranes was blocked with 5% non-fat milk, probed with specific primary antibodies at 4 °C overnight, then incubated with secondary HRP-linked antibody for one hour at room temperature. Blots were visualized using EZ-ECL detection kit for HRP (Biological Industries) and signals were photographed by Chemi XRQ Imaging System (Gene Company Limited). Quantitative density analysis of blots was calculated using ImageJ 1.45S software (National Institutes of Health). And the original figures of Western Blot design of this study were shown in Fig. S1.

2.11. In Vivo *CRC Xenograft Studies*

All the following animal experiments were approved by the animal ethics committee of Zhejiang Chinese Medical University (IACUC-20200330-01). 5×10^5 LS-174T or HT-29 cells suspended in 100 μL PBS were subcutaneously implanted into the right flank of 3 or 4-weeks-old female nude mice purchased and maintained in Zhejiang Chinese Medical University to construct subcutaneous tumor models. Treatments began at one week post-implantation when the tumor volume reached approximately 30 mm^3 (V = length x $width^2/2$), and tumor-bearing mice were randomly divided into two groups ($n = 7$). The treatment consisted of five intratumoral injections of Opti-MEM or virus (1×10^7 PFU/dose) in 100 μL volume, on post-implantation days 7,8,9,10,11 on LS-174T tumor models and days 7,9,11,13, 15 on HT-29 tumor models. For animal survival, tumor burden was measured using vernier caliper every two or three days. Mice were euthanized when diameter reached approximately 1.5 cm in any direction, body weight decreased by 20%, natural death or tumor burst and necrosis occurred.

Tumor tissues ($n = 3$) were collected three days after the last injection for the subsequent experiments. For frozen section, excised tumors were rapidly refrigerated to a certain degree of hardness to make 4 μm slices and the green fluorescence generated by rMV-Hu191-H-EGFP was monitor under microscope (Zeiss Observer. Z1). Freshly excised tumor tissues were fixed in 4% formalin and embedded in paraffin for hematoxylin-eosin staining. As for immunohistochemistry, paraffin-embedded sections were dewaxed with xylene, hydrated in gradient ethanol, repaired antigen, blocked with normal serum, and then incubated with the indicated primary and secondary antibody.

2.12. Statistical analysis

Student's t test and one-way multiple comparisons (ANOVA) were utilized to assess statistical significance by GraphPad Prism version 6.0. Animal survival was statistically analyzed using Kaplan-Meier survival curves and log-rank test. All data exhibited representatively above were repeated at least three times and presented as mean ± SD. P value below 0.05 was considered to have statistical differences. $^{*}P < 0.05$; $^{**}P < 0.01$; $^{***}P < 0.001$; $^{****}P < 0.0001$.

3. Results

3.1. Abundance of CD46, Nectin-4 in human CRC cell lines' surface

CD46 is considered to be pivotal in mediating MV vaccine strain's entrance to tumor cells [13,28]. It was extremely highly expressed in a series of CRC cells with 99.8% in LS-174T, 99.9% in HT-29, 99.9% in SW620, 99.9% in HCT-116, and 97.2% in DLD-1, while Nectin-4 expression was much lower with 9.29% in LS-174T, 44% in HT-29, 2.96% in SW620, 0.21% in HCT-116 and 60.4% in DLD-1(Fig. 1A).

3.2. rMV-Hu191 induced efficient infection and oncolytic effects in human CRC cell lines

The green fluorescence generated by virus replication between adjacent cells was observed at 48 h post infection with a dose-dependence manner (Fig. 1B). As shown in Fig. 1C, the cytopathic effects of rMV-Hu191-H-EGFP in CRC cell lines at 72 h post infection was a MOI gradient dependence as well. The proliferation ability and cytotoxicity of rMV-Hu191-H-EGFP in CRC cell lines were demonstrated with dose and time-dependent manners by CCK8 assay (Fig. 1D). In order to investigate the cytotoxicity of rMV-Hu191-H-EGFP on normal cells, we detected the cell viability of HUVEC cells after virus infection. As shown in Fig. 1E, rMV-Hu191-H-EGFP could also kill HUVEC cells to a certain extent, but a higher MOI was demanded to execute a weaker inhibition of cell growth compared to CRC cells. Furthermore, the virus growth kinetics was quantified by TCID50 assay, by which the titers of virus progeny particles also followed dose and time-dependent manners (Fig. 1F).

3.3. The caspase-dependent apoptosis induced by rMV-Hu191 infection

As shown in Fig 2A, the apoptotic proportion of cells infected with rMV-Hu191 was dramatically increased with a time-dependence manner. In LS-174T cells, the proportion of apoptotic cells at 24 h, 36 h, 48 h and 60 h post infection was 29%, 40.8%, 43.7% and 50.1%, respectively, compared with 4.8% in the control group. And in HT-29 cells, the proportion of apoptotic cells at 24 h, 36 h, 48 h and 60 h post infection

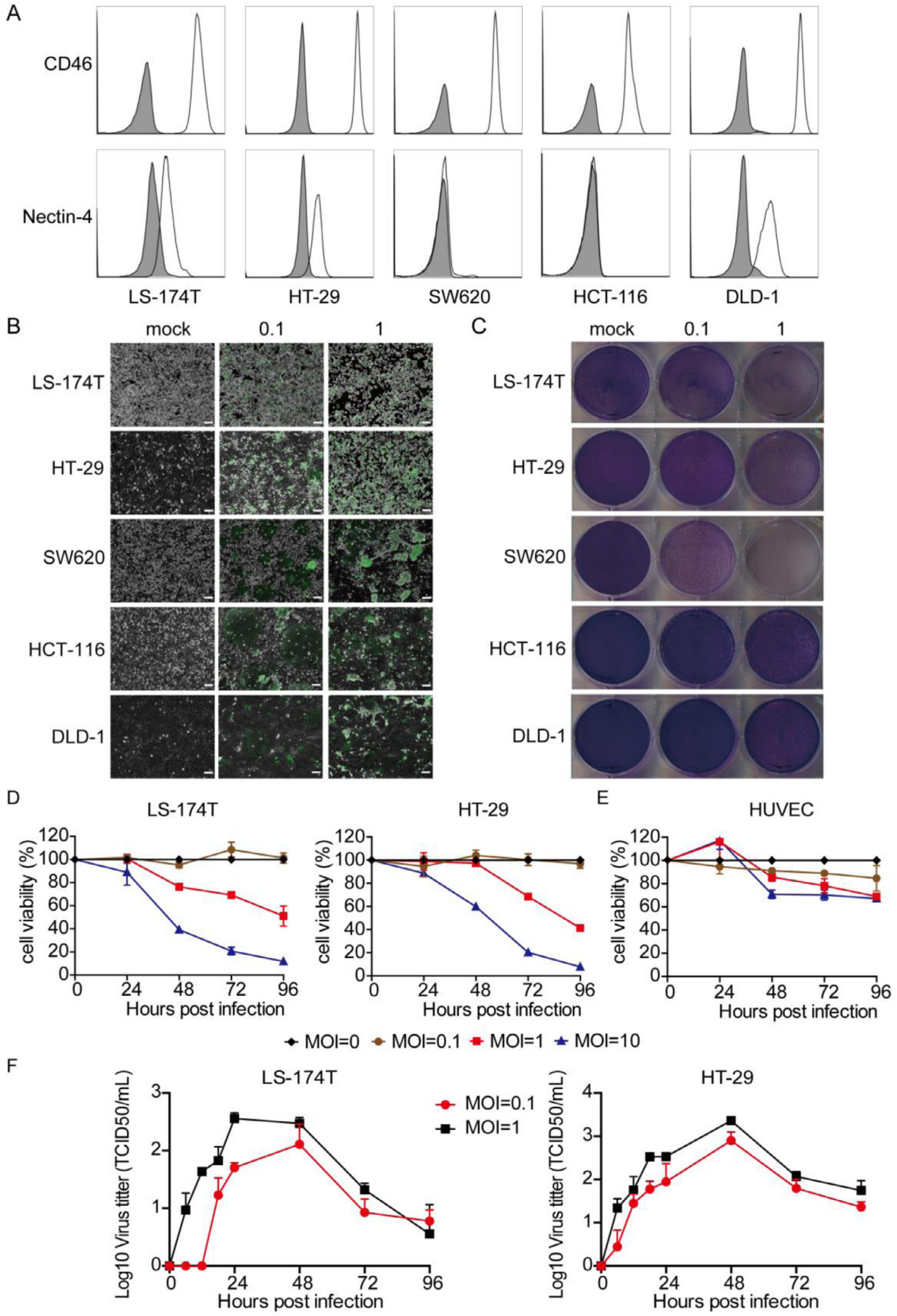

Fig. 1. *In vitro* infection and cytotoxicity of rMV-Hu191 in human CRC cells.
(A) A panel of human CRC cells was determined by flow cytometry for the measles virus receptors, CD46 and Nectin-4. Isotype control staining was shown as solid histograms, while CD46 or Nectin-4 staining was shown as shaded histograms. (B) The green fluorescence in virus typical syncytia formed by rMV-Hu191-H-EGFP at 48 h post infection was monitored by fluorescence microscopy. Scale bar, 100 μm. (C) Virus-induced cytotoxic effects at 72 h post infection exhibited by crystal violet staining. (D, E) Cell viability was assessed by CCK8 Assay every 24 h post infection at multiple MOIs. Data were presented as mean ± SD from three repeated experiments. (F) Cells infected with virus were collected at indicated times and concentrations. Offspring virus particles were titered by TCID50 assay to perform viral growth kinetics.

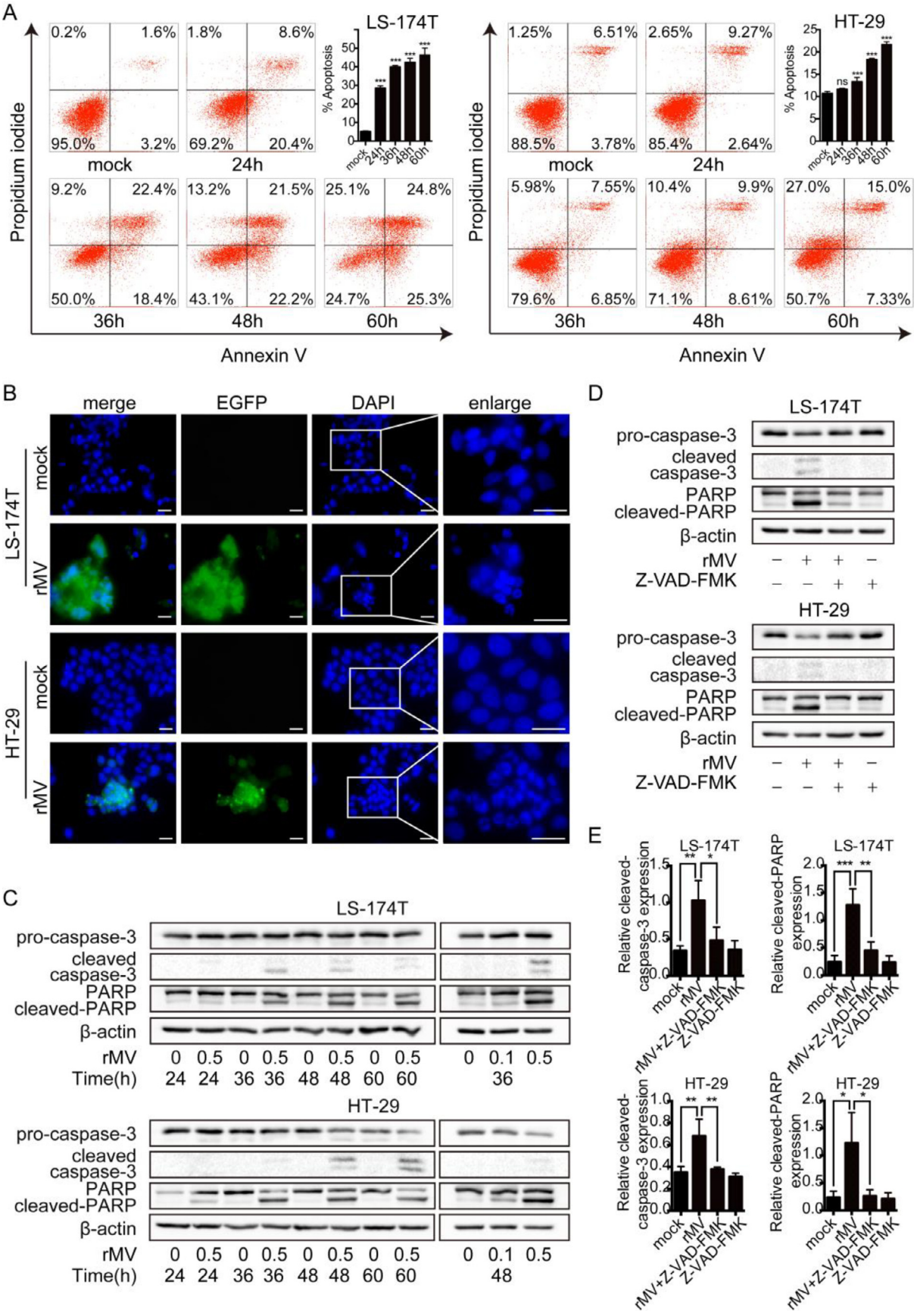

Fig. 2. rMV-Hu191 promoted apoptosis via the caspase-dependent pathway in human CRC cells.
(A) The CRC cells were treated with rMV-Hu191 at MOI = 0.5, and the percentage of apoptotic cells was analyzed at indicated times by flow cytometry using an apoptosis kit. Representative results from three independent experiments were shown as mean ± SD. $^{***}P < 0.001$. (B) Cells infected with rMV-Hu191-H-EGFP at MOI = 0.5 were stained with DAPI solution. Then the co-localizations of nuclear fragmentation and virus-generated green fluorescence were photographed under a fluorescent microscope. Scale bar, 20 μm. (C) Activation of apoptotic marker proteins, cleaved-caspase-3 and cleaved-PARP at indicated times and concentrations was determined by Western blot assay. (D) Expression levels of cleaved-caspase-3 and cleaved-PARP after co-treatment with rMV-Hu191-H-EGFP (MOI = 0.5) and Z-VAD-FMK (100 μM) for 48 h were assessed by Western blot assay. (E) Quantification of the relative cleaved-caspase-3 and cleaved-PARP ratio was presented. Data were representative of three independent experiments and were shown as mean ± SD. $^{*}P < 0.05$; $^{**}P < 0.01$; $^{***}P < 0.001$.

was 11.91%, 14.4%, 18.51% and 22.33%, compared with 10.29% in the mock group. Treating human CRC cells with rMV-Hu191-H-EGFP led to characteristic morphological changes of apoptosis, such as nuclear fragmentation (Fig. 2B) by DAPI staining co-localized with virus.

The activation levels of caspase-3 and PARP which were the end-executing protein of apoptosis and its substrate, were examined by Western blot assay. Along with the dose and time manners of virus infection, the activation of cleaved-caspase-3 and cleaved-PARP was significantly increased at the same time (Fig. 2C). Then, CRC cells were co-cultured with rMV-Hu191-H-EGFP and Z-VAD-FMK (a pan-caspase inhibitor). The result displayed that the activation of cleaved caspase-3 and cleaved-PARP was dramatically abolished with statistical significance (Fig. 2D, E). In conclusion, the above results further clarified that rMV-Hu191-induced apoptosis was caspase-dependent in CRC cells.

3.4. rMV-Hu191 induced complete autophagy and promoted autophagy flux in CRC cells

As shown in Fig. 3A, the conversion and lipidation of LC3B-I to LC3B-II were obviously increased and the expression of p62 was evidently reduced in the rMV-Hu191-H-EGFP-treated group, which were both in time and dose-dependent manners. To further elucidate virus-induced autophagy, numerous green fluorescent puncta (Fig. 3B) were examined in typical syncytia formed by rMV-Hu191 in LS-174T and HT-29 cells stably expressing LC3B-EGFP. Then transmission electron microscopy (TEM) was applied to monitor autophagosomes formation after rMV-Hu191-H-EGFP treatment. We observed a mass of classical double-membrane autophagosomes in cytoplasm of the treated group compared with the control group (Fig. 3C).

However, LC3B-I to LC3B-II conversion does not always necessarily indicate autophagy up-regulation because lysosomal inhibition causes the same results while it rather inhibits autophagy. For this objective, we monitored autophagy flux by western blotting using lysosomal inhibitor CQ. As shown in Fig. 3D, the autophagy flux in virus-treated group accompanied by CQ was obviously blocked with the increase of LC3B-II and p62. With the purpose to further illuminate autophagosomes accumulation treated with rMV-Hu191, CRC cells stably expressing LC3B-EGFP, were labeled with LysoTracker Red, which was an eosinophilic fluorescent probe used to mark and trace acidic organelles in live cells. LC3B-EGFP and LysoTracker Red co-localized after virus infection (Fig. 3E), which was more evident with the known autophagy activator Rapa treatment. These data were consistent with the western blotting results of p62 decrease, suggesting that autophagosomes and lysosomes fused together to form autolysosomes to promote the progress of autophagy flux after rMV-Hu191 infection.

3.5. Autophagy served as a protective role in rMV-Hu191-induced apoptosis in human CRC cells

Since autophagy was a double-edged sword of cell fate, the complicated relationships between autophagy and apoptosis varied with cell types and stimulus factors [29]. To gain further insight into the role of autophagy played in the rMV-Hu191-H-EGFP-induced apoptosis in LS-174T cells, we used Rapa, an activator with activity against mTOR, to promote autophagy. And ATG7, a gene involved in the initiation of autophagosomes formation, was knocked down by shATG7 to inhibit autophagy.

Our results revealed that the ratio of rMV-Hu191-H-EGFP-induced apoptosis was significantly inhibited by Rapa treatment (Fig. 4A, B, C, D, E) with the obviously decrease of cleaved-caspase-3 and cleaved-PARP. Meanwhile, the suppression of autophagy by shATG7 markedly enhanced rMV-Hu191-H-EGFP-induced apoptosis (Fig. 4F, G, H, I, J, K) with the dramatically increase of cleaved-caspase-3 and cleaved-PARP. It has been reported that ATG7 could promote viral replication, which might be related to the phenotype shown in this study. Therefore, we examined viral growth on LS-174T cells and LS-174T cells stably transfected with shATG7, and found no difference (Fig. S2). Taken together, our results demonstrated that autophagy played a protective role in rMV-Hu191-induced apoptosis in human CRC cells.

3.6. PI3K/AKT signaling pathway regulated rMV-Hu191-induced autophagy and apoptosis in human CRC cells

Since PI3K/AKT is one of the common upstream pathways of autophagy and apoptosis, we detected the phosphorylation of key kinases to figure out whether rMV-Hu191-H-EGFP triggered the PI3K/AKT pathway in LS-174T cells. As shown in Fig. 5A, the level of phosphorylated AKT^{Ser473} ($p\text{-}AKT^{Ser473}$) was obviously accumulated with a dose-dependent manner infected with virus compared to respective controls, while total protein without obvious changes. And expression of PTEN was markedly reduced. These data suggested that rMV-Hu191-H-EGFP activated the PI3K/AKT pathway in LS-174T cells.

We next explored the connection of PI3K/AKT signaling pathway with rMV-Hu191-H-EGFP-induced autophagy and apoptosis in absence or presence of the PI3K inhibitor LY294002. As shown in Fig. 5B and C, LY294002 effectively downregulated the expression levels of $p\text{-}AKT^{Ser473}$ ($P < 0.01$). In presence of LY294002, rMV-Hu191-H-EGFP-induced autophagy was significantly decreased ($P < 0.05$, Fig. 5D, E). And rMV-Hu191-H-EGFP-induced apoptosis was obviously increased accompanied by LY294002 treatment ($P < 0.01$, Fig. 5F, G, H). Taken together, we concluded that the activation of PI3K/AKT pathway promoted rMV-Hu191-H-EGFP-induced autophagy and suppressed rMV-Hu191-H-EGFP-induced apoptosis.

3.7. Tumor regression effects of rMV-Hu191 in human CRC xenografts

To confirm *in vivo* oncolytic effects of rMV-Hu191-H-EGFP, nude mice bearing subcutaneous human CRC tumors were applied intratumoral virus injection to assess the antitumor efficacy. The injections of rMV-Hu191-H-EGFP resulted in growth suppression of tumor volume (Fig. 6A, B) in LS-174T ($P < 0.05$) and HT-29 ($P < 0.01$) xenografts compared to the mock group treated with equivalent dose of Opti-MEM. The median survival was 18 days in treated group and 9 days in control group ($P < 0.01$) in LS-174T xenografts, while 39 days in treated group and 30 days in control group in HT-29 xenografts ($P < 0.001$) (Fig. 6C). These data indicated that rMV-Hu191-H-EGFP had potent antitumor effects and prolonged the survival of human CRC xenografts significantly.

Three days after the last injection, animals ($n = 3$) were sacrificed to harvest tumor tissues. The green fluorescence (Fig. 6D) and measles virus-nucleoprotein (Fig. 6E) were observed in the frozen sections of tumors inoculated with virus but not in the control group, proving the existence of virus. Morphologically, HE staining sections showed large areas of necrosis and swelling of apoptotic cells in the virus-treated group (Fig. 6F). The results from IHC staining showed the increased expression of cleaved-caspase-3 (Fig. 6G) and LC3B (Fig. 6H) in virus-treated tumor tissues. Similarly, the protein levels of cleaved-caspase-3 and LC3B extracted from virus-treated groups also exceeded the control groups (Fig. 6I and J).

4. Discussion

The emerging oncolytic virotherapy is expected to be the next prime breakthrough in tumor therapy. To date, extensive OVs display remarkable efficacy in inhibition of tumorigenesis, and have been admitted into clinical trials, including measles virus [30,31], adenovirus [32], herpes simplex virus-1 [33], vaccinia virus [34] and so forth. The Chinese attenuated measles vaccine strain rMV-Hu191, authorized by the Chinese government with long history of vaccination and guaranteed security, is a promising candidate for oncolytic virotherapy. In this study, we had firstly certified that rMV-Hu191 could serve as an oncolytic virotherapy candidate for human CRC.

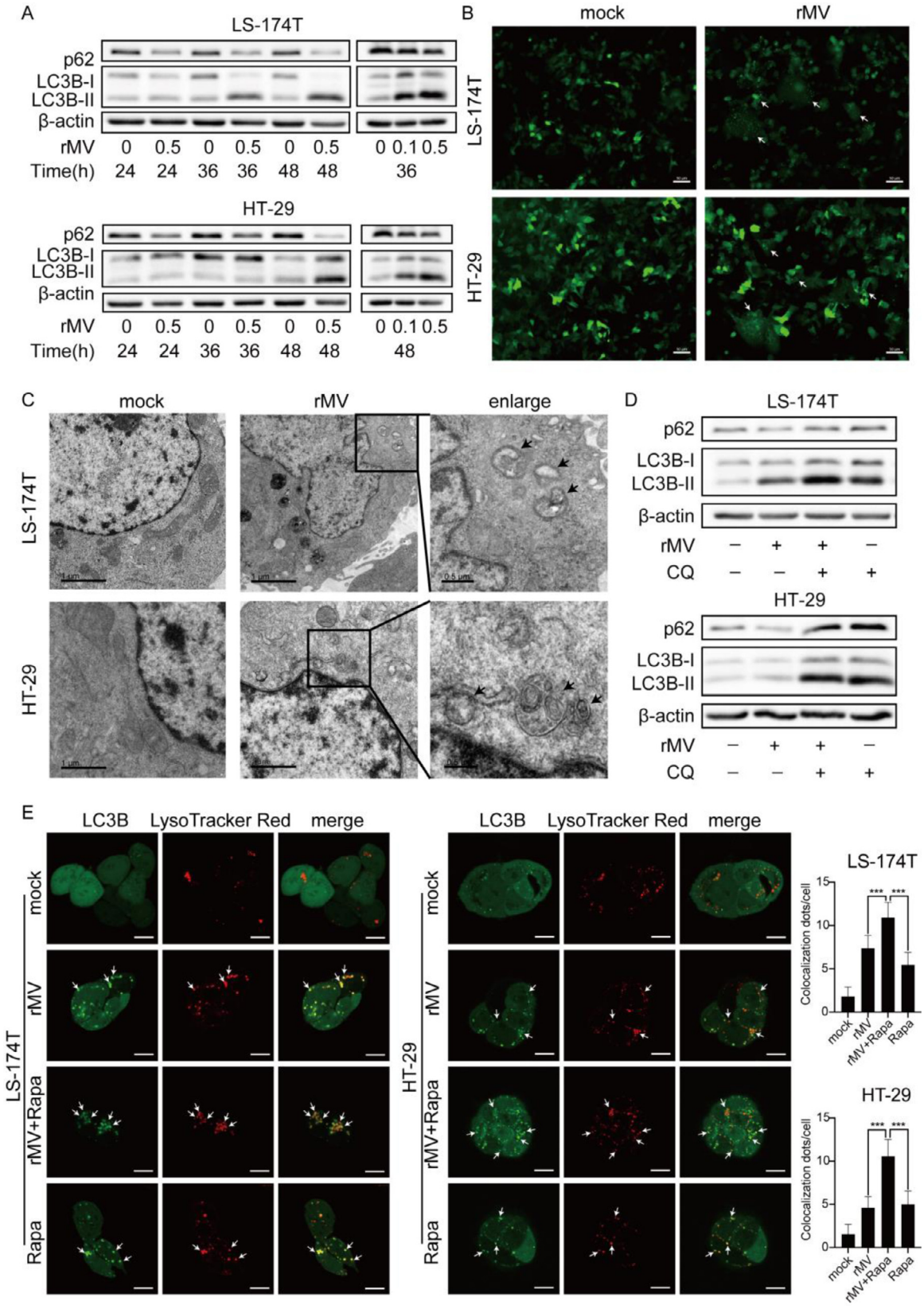

Fig. 3. Complete autophagy induced by rMV-Hu191 in human CRC cells.

(A) Conversion of LC3B-I to LC3B-II and decrease of p62 in CRC cells treated with rMV-Hu191-H-EGFP (MOI = 0.5) at indicated times (left panel) and concentrations (right panel). (B) Cells stably expressing LC3B-EGFP were exposed to rMV-Hu191 (MOI = 0.5) for 1.5 h. The conversion and lipidation of LC3B-I (cytoplasm distribution) to LC3B-II (autophagosomes membrane distribution, green dots, white arrows) were photographed by an inverted fluorescence microscopy at 36 h post infection. Bars represent 50 μm. (C) The formation of autophagosomes (black arrows) which were structures with double layer containing intracellular contents was observed by TEM in rMV-Hu191-H-EGFP-infected cells. (D) The expression levels of LC3B-II and p62 in CRC cells infected with rMV-Hu191-H-EGFP (MOI = 0.5) accompanied by CQ treatment (20 μM) for 36 h. (E) Autophagosomes fuse with lysosomes in virus-infected cells. Cells co-treated with rMV-Hu191 (MOI = 0.5) and Rapa (3 μM) for 36 h, were incubated with LysoTracker Red (50 nM) for 30 min. The co-localizations of LC3B-EGFP-labeled autophagosomes (green) and LysoTracker Red-labeled acid vesicles (red) were determined using a confocal microscopy (white arrows). Bars represent 10 μm.

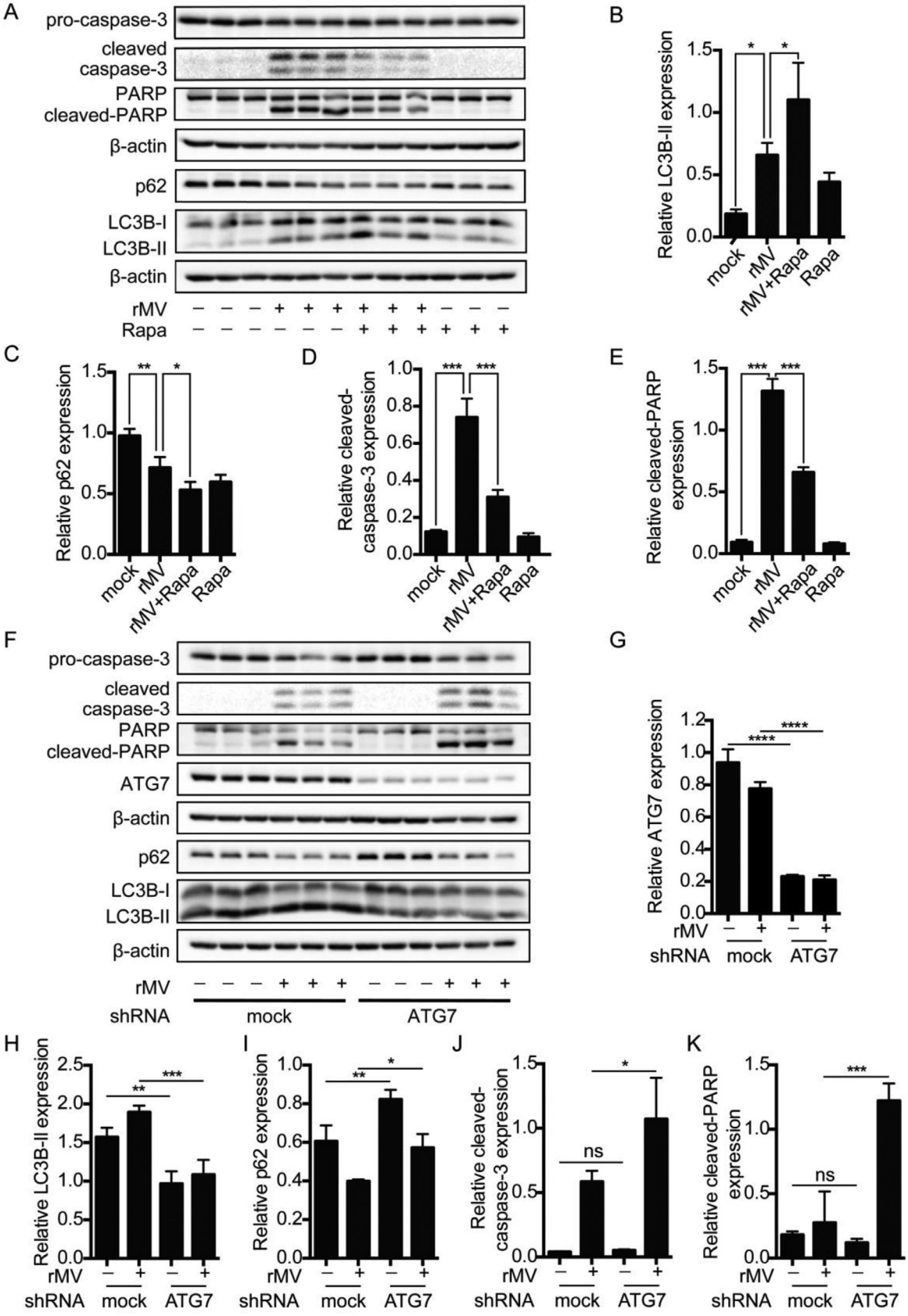

Fig. 4. Autophagy served as a protective role in human CRC cells' apoptosis generated by rMV-Hu191.
(A) Western blotting results of LS-174T cells treated with rMV-Hu191-H-EGFP at MOI = 0.5 in the absence or presence of Rapa (3 μM) for 36 h. Densitometry analysis of the protein levels of LC3B-II (B), p62 (C), cleaved-caspase-3 (D) and cleaved-PARP (E). (F) LS-174T cells knocked down by shATG7 or sh.mock were followed with rMV-Hu191-H-EGFP treatment (MOI = 0.5, 36 h). Densitometry analysis of the protein levels of ATG7 (G), LC3B-II (H), p62 (I), cleaved-caspase-3 (J), and cleaved-PARP (K). *, compared with sh.mock cells. Similar consequences were obtained in three independent trials for densitometry analysis. $^{*}P < 0.05$; $^{**}P < 0.01$; $^{***}P < 0.001$.

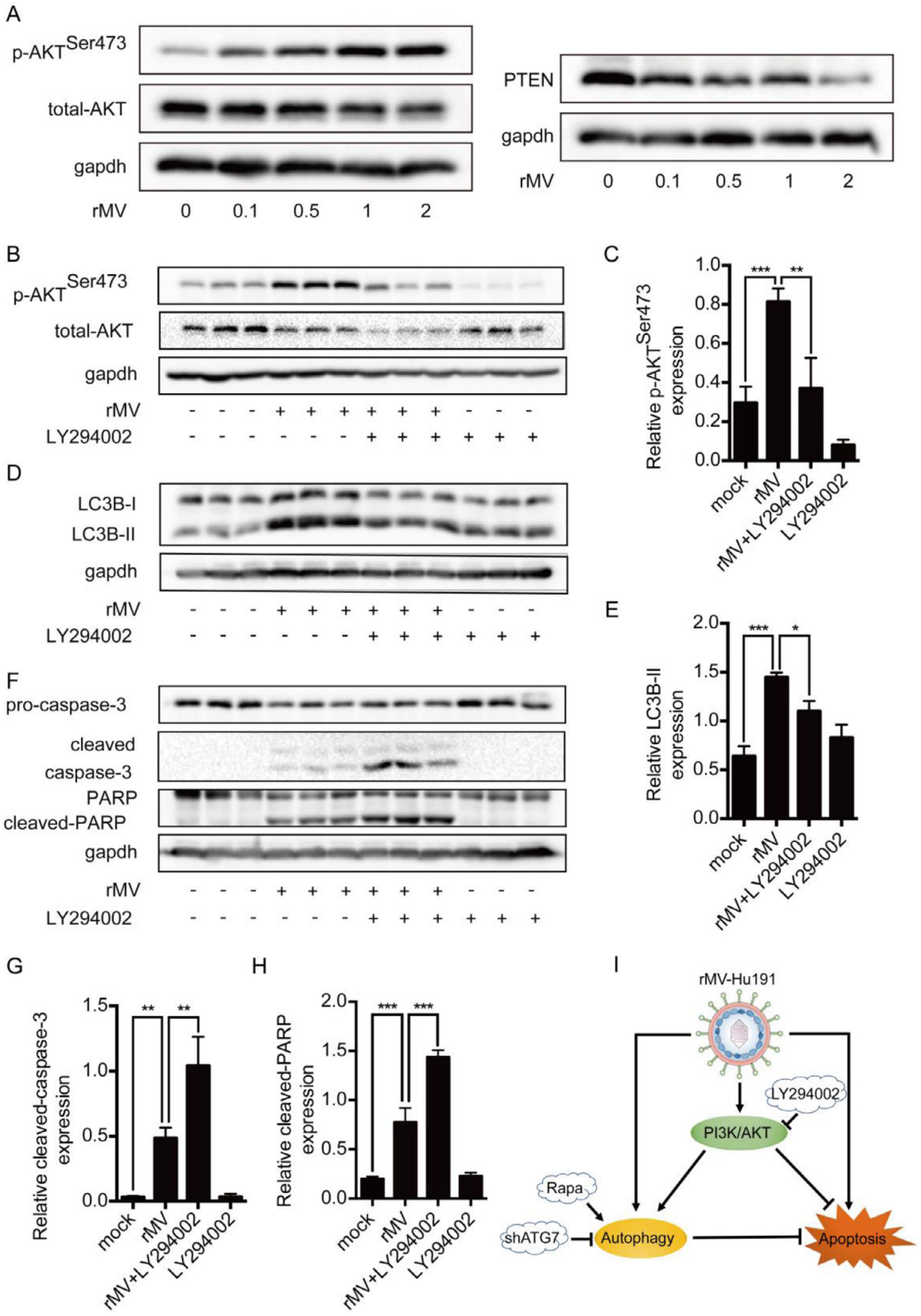

Fig. 5. PI3K/AKT signaling pathway regulated rMV-Hu191-induced apoptosis and autophagy.
(A) Expression levels of p-AKT^{Ser473}, total-AKT and PTEN in LS-174T cells treated with rMV-Hu191-H-EGFP at indicated concentrations for 36 h. Expression levels of p-AKT^{Ser473} (B), autophagy marker proteins (D) and apoptosis marker proteins (F) in LS-174T cells treated with virus (MOI = 0.5), with or without LY294002 (25 μM) for 36 h. Densitometry analysis of proteins levels of p-AKT^{Ser473} (C), LC3B-II (E), cleaved-caspase-3 (G), and cleaved-PARP (H). (I) A schematic diagram: the connection of the PI3K/AKT signaling pathway and rMV-Hu191-induced autophagy and apoptosis. All Western blotting data were obtained from three independent experiments. $^{*}P < 0.05$; $^{**}P < 0.01$; $^{***}P < 0.001$.

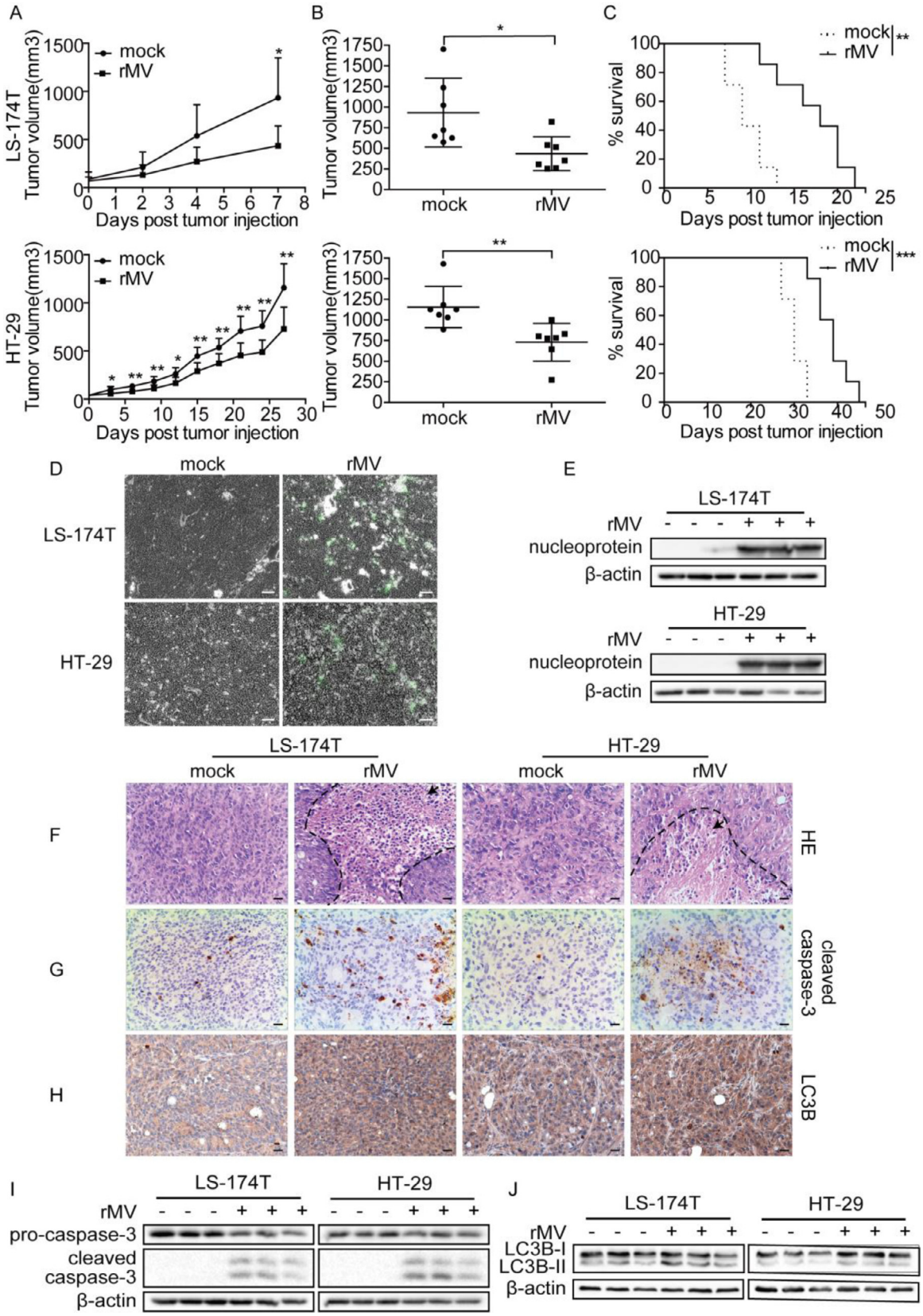

Fig. 6. The oncolytic effect of rMV-Hu191 in human CRC xenografts.

(A) Tumor burden of human CRC xenografts with or without intratumoral injections of rMV-Hu191-H-EGFP was monitored every two or three days. (B) Distributions of tumor volumes on day 7 and day 27 post injection in LS-174T xenografts and HT-29 xenografts. Dots represented tumor volume of individual mice ($n = 7$). (C) The survival of tumor-bearing mice was supervised by Kaplan-Meier analysis and statistical difference was administrated with log-rank test ($n = 7$). Detections of green fluorescence (D) and MV-nucleoprotein (E) generated by virus *in vivo*. Bars represent 100 μm. Paraffin-embedded tumor sections were stained with HE for evaluating cells morphological changes (F, black arrows) and IHC staining for evaluating apoptosis (G) and autophagy (H) changes with virus treatment *in vivo*. Bars represent 50 μm. (I and J) Expression of cleaved-caspase-3 and LC3B in tumor tissues from rMV-Hu191 and mock treated mice. Data were shown as mean ± SD, ($n = 3$). $^{*}P < 0.05$; $^{**}P < 0.01$; $^{***}P < 0.001$.

Programmed cell death (PCD) including apoptosis, autophagy and necrosis [35], known as a generally cellular self-destroying process to dislodge damaged cells and maintain an endogenous homeostasis under certain emergencies, including tumorigenesis. Based on the above, PCD constitutes a promising target for tumor elimination. Apoptosis, known as type I PCD, is the extensively well-defined one. From our data, we had determined that rMV-Hu191 induced effective antitumor activity and triggered apoptotic cell death in CRC cells with minor cytotoxicity in normal HUVEC cells. We found that rMV-Hu191 induced augment of cleaved-caspase-3 and cleaved-PARP, the two apoptotic marker proteins, which could be abolished by the pan-caspase inhibitor Z-VAD-FMK, suggesting that rMV-Hu191 induced the caspase-dependent apoptosis in human CRC cells.

Autophagy is a process long known as a survival advantage to envelope and degrade damaged-organelles by forming autophagosomes to hold cellular homeostasis for cells undergoing context stresses. It has been recognized as type II PCD [36]. However, excessive or insufficient activation of autophagy both could cause cell death. In general, the character of autophagy whether promoting cell survival or resulting cell death is exceedingly context dependent. LC3B-II, serves as a crucial mark protein of autophagy, is lipidated from LC3B-I and participates in autolysosomes formation [37]. p62, an ubiquitinated substrate transferred from autophagosomes to autolysosomes reflecting the continuous and dynamic process of autophagy flux, is recognized as an autophagy negative marker [38]. And there were two mechanisms for the augments of autophagosomes: one was the accumulation of autophagosomes formation accompanied with p62 decrease, called complete autophagy; the other was the blockage of autophagosomes maturation accompanied with p62 increase, called incomplete autophagy. In this article, we had demonstrated that rMV-Hu191 accelerated the LC3B-II lipidation, and markedly decreased the p62 expression level. The autophagosomes and autolysosomes, which were double membrane structures wrapped cytoplasmic material, had been detected by transmission electron microscopy. We gained further insight to rMV-Hu191-induced autophagic flux via the lysosomal inhibitor CQ and the co-localization of LC3B-EGFP and lysosomes by confocal microscopy. These data strongly suggested that rMV-Hu191 promoted complete autophagy in human CRC cells.

Autophagy and apoptosis, as two evolutionarily conserved processes, are crucial to regulate cell fate under various stresses [39]. The crosstalk between these two processes is very complicated and sometimes even contradictory. Autophagy is considered as a stress adaptation and cytoprotective mechanism to escape apoptosis-induced cell death. Under certain conditions, it is also identified as an autophagic-cell death pathway [40]. Thus, it is necessary to figure out the complex interplay of autophagy and apoptosis following different treatments. Deal with the specific autophagy promotor Rapa prominently decreased the expression level of apoptosis proteins, whereas knockdown of ATG7, a gene involved in the initiation of autophagosomes formation by shRNA remarkably increased the rMV-Hu191-induced apoptosis. These results suggested that autophagy exist as a temporary self-protective mechanism against rMV-Hu191-induced apoptosis, and provided new insight into the autophagy as a potential intervention strategy for upregulating apoptosis in tumor therapy.

Previous studies have revealed that PI3K/AKT pathway as one of the common upstream signaling pathway of apoptosis, autophagy and proliferation, is frequently dysregulated in cancers pathogenesis. Our data had proved that rMV-Hu191 obviously activated the PI3K/AKT pathway with dose-dependent manner in CRC cells. In addition, utilization of PI3K inhibitor LY294002 inhibited rMV-Hu191-induced autophagy, whereas promoted rMV-Hu191-induced apoptosis. To assess the oncolytic efficacy of rMV-Hu191 *in vivo*, we constructed human CRC xenograft nude models. As our results shown, the intratumoral injection of rMV-Hu191 generated remarkable tumor suppression and prolonged animal survival time with statistical significance. It is well known that measles virus cannot infect mice because of lacking viral receptors [41]. Side effects and other reactions induced by rMV-Hu191 need to be assessed in transgenic mice or primates. And a major barrier to the effectively systemic delivery of oncolytic measles viruses as antitumor agents is the anti-measles neutralizing antibodies pre-existing in vaccinated individuals. It is prospective that these problems could be addressed by combining immunosuppressive drugs transiently depleting anti-measles antibodies prior to therapy [42], using measles-infected cell carriers to deliver the virus [43,44], and engineering oncolytic measles viruses evading be neutralized by anti-measles antibodies [45].

In conclusion, our data demonstrated that recombinant Chinese measles virus vaccine strain rMV-Hu191 generated tumor therapeutic efficacy in human CRC both *in vitro* and *in vivo*. rMV-Hu191 induced caspase-dependent apoptosis and complete autophagy, and activated the PI3K/AKT pathway. And autophagy served as a protective role in rMV-Hu191-induced apoptosis. PI3K/AKT pathway regulated this two processes by promoting rMV-Hu191-induced autophagy and inhibiting rMV-Hu191-induced apoptosis (Fig. 5I). And in order to detect whether inhibitors play a direct role on virus replication, we also measured the virus growth curves in LS-174T cells treated with rMV-Hu191 and inhibitors used in this study and found no statistical difference (Fig. S3). Taken together, in this study, we well explain the relationship between rMV-Hu191-induced apoptosis, autophagy and the PI3K/AKT pathway. And the underlying mechanisms may provide us a theoretical basis for applying this attenuated measles virus as an innovative oncolytic agent against human CRC, such as combinational therapy of rMV-Hu191 with agents targeting autophagy or PI3K/AKT pathway.

Author contributions

Chu-di Zhang: Conceptualization, Methodology, Data curation, Formal analysis, Writing-original draft, Writing-review & editing. Dongming Zhou: Methodology, Formal analysis. Yao Lv: Writing-review & editing. Yi-long Wang: Supervision. Meng-ying Zhu: Validation. Qiaoqiang Hao: Investigation. Chu-fan Qu: Data curation. Yi Chen: Data curation. Wei-zhong Gu: Methodology. Ben-qing Wu: Methodology. Peichun Chen: Methodology. Zheng-yan Zhao: Conceptualization, Funding acquisition, Writing-review & editing.

Funding

This work was supported by the Zhejiang Provincial Science technology research program (2017C33047).

Abbreviations

rMV-Hu191: recombinant Chinese measles virus vaccine strain Hu191; CRC: human colorectal cancer; OVs: oncolytic viruses; MV: measles virus; TCID 50: tissue culture infective dose; MOI: multiplicity of infection; ATG: autophagy related genes; ATCC: American Type Culture Collection; PFU: plaque forming unit assay; CCK8: Cell Counting Kit-8 assay.

Author contribution statement

Chu-di Zhang: Conceptualization, Methodology, Data curation, Formal analysis, Writing-original draft, Writing-review & editing. Dongming Zhou: Methodology, Formal analysis. Yao Lv: Writing-review & editing. Yi-long Wang: Supervision. Meng-ying Zhu: Validation. Qiaoqiang Hao: Investigation. Chu-fan Qu: Data curation. Yi Chen: Data curation. Wei-zhong Gu: Methodology. Ben-qing Wu: Methodology. Peichun Chen: Methodology. Zheng-yan Zhao: Conceptualization, Funding acquisition, Writing-review & editing.

Declaration of Competing Interest

No conflicts of interest.

References

[1] F. Bray, J. Ferlay, I. Soerjomataram, R.L. Siegel, L.A. Torre, A. Jemal, Global cancer statistics 2018: GLOBOCAN estimates of incidence and mortality worldwide for 36 cancers in 185 countries, CA Cancer J. Clin. 68 (2018) 394–424.

[2] H. Brody, Colorectal cancer, Nature 521 (2015) S1.

[3] E. Dekker, P.J. Tanis, J.L.A. Vleugels, P.M. Kasi, M.B. Wallace, Colorectal cancer, Lancet 394 (2019) 1467–1480.

[4] N.H. Goradel, N. Mohajel, Z.V. Malekshahi, S. Jahangiri, M. Najafi, B. Farhood, K. Mortezaee, B. Negahdari, A. Arashkia, Oncolytic adenovirus: a tool for cancer therapy in combination with other therapeutic approaches, J. Cell. Physiol. 234 (2019) 8636–8646.

[5] X.Q. Liu, H.Y. Xin, Y.N. Lyu, Z.W. Ma, X.C. Peng, Y. Xiang, Y.Y. Wang, Z.J. Wu, J.T. Cheng, J.F. Ji, J.X. Zhong, B.X. Ren, X.W. Wang, H.W. Xin, Oncolytic herpes simplex virus tumor targeting and neutralization escape by engineering viral envelope glycoproteins, Drug Deliv. 25 (2018) 1950–1962.

[6] X. Meng, T. Nakamura, T. Okazaki, H. Inoue, A. Takahashi, S. Miyamoto, G. Sakaguchi, M. Eto, S. Naito, M. Takeda, Y. Yanagi, K. Tani, Enhanced antitumor effects of an engineered measles virus Edmonston strain expressing the wild-type N, P, L genes on human renal cell carcinoma, Mole. Ther. 18 (2010) 544–551.

[7] M. Zeyaullah, M. Patro, I. Ahmad, K. Ibraheem, P. Sultan, M. Nehal, A. Ali, Oncolytic viruses in the treatment of cancer: a review of current strategies, Pathol. Oncol. Res. 18 (2012) 771–781.

[8] F. Huang, B.R. Wang, Y.Q. Wu, F.C. Wang, J. Zhang, Y.G. Wang, Oncolytic viruses against cancer stem cells: A promising approach for gastrointestinal cancer, World J. Gastroenterol. 22 (2016) 7999–8009.

[9] N. Cifuentes-Munoz, F. El Najjar, R.E. Dutch, Viral cell-to-cell spread: conventional and non-conventional ways, Adv. Virus Res. 108 (2020) 85–125.

[10] A. Dispenzieri, C. Tong, B. LaPlant, M.Q. Lacy, K. Laumann, D. Dingli, Y. Zhou, M.J. Federspiel, M.A. Gertz, S. Hayman, F. Buadi, M. O'Connor, V.J. Lowe, K.W. Peng, S.J. Russell, Phase I trial of systemic administration of Edmonston strain of measles virus genetically engineered to express the sodium iodide symporter in patients with recurrent or refractory multiple myeloma, Leukemia 31 (2017) 2791–2798.

[11] S. Aref, K. Bailey, A. Fielding, Measles to the rescue: a review of oncolytic measles virus, Viruses 8 (2016).

[12] R.S. Noyce, D.G. Bondre, M.N. Ha, L.T. Lin, G. Sisson, M.S. Tsao, C.D. Richardson, Tumor cell marker PVRL4 (nectin 4) is an epithelial cell receptor for measles virus, PLoS Pathog. 7 (2011) e1002240.

[13] H. Tatsuo, N. Ono, K. Tanaka, Y. Yanagi, SLAM (CDw150) is a cellular receptor for measles virus, Nature 406 (2000) 893–897.

[14] N. Dhiman, R.M. Jacobson, G.A. Poland, Measles virus receptors: SLAM and CD46, Rev. Med. Virol. 14 (2004) 217–229.

[15] Y. Wang, R. Liu, M. Lu, Y. Yang, D. Zhou, X. Hao, D. Zhou, B. Wang, J. Li, Y.W. Huang, Z. Zhao, Enhancement of safety and immunogenicity of the Chinese Hu191 measles virus vaccine by alteration of the S-adenosylmethionine (SAM) binding site in the large polymerase protein, Virology 518 (2018) 210–220.

[16] D. Zhou, M.Y. Zhu, Y.L. Wang, X.Q. Hao, D.M. Zhou, R.X. Liu, C.D. Zhang, C.F. Qu, Z.Y. Zhao, Attenuated MuV-S79 as vector stably expressing foreign gene, World J. Pediatr. 15 (2019) 511–515.

[17] D. Zhou, M.Y. Zhu, Y.L. Wang, X.Q. Hao, D.M. Zhou, R.X. Liu, C.D. Zhang, C.F. Qu, Z.Y. Zhao, Establishment of an efficient reverse genetic system of Mumps virus S79 from cloned DNA, World J. Pediatr. 15 (2019) 499–505.

[18] Y. Lv, D. Zhou, X.Q. Hao, M.Y. Zhu, C.D. Zhang, D.M. Zhou, J.H. Wang, R.X. Liu, Y.L. Wang, W.Z. Gu, H.Q. Shen, X. Chen, Z.Y. Zhao, A recombinant measles virus vaccine strain rMV-Hu191 has oncolytic effect against human gastric cancer by inducing apoptotic cell death requiring integrity of lipid raft microdomains, Cancer Lett. 460 (2019) 108–118.

[19] N.N. Danial, S.J. Korsmeyer, Cell death: critical control points, Cell 116 (2004) 205–219.

[20] D.J. Klionsky, The molecular machinery of autophagy: unanswered questions, J. Cell. Sci. 118 (2005) 7–18.

[21] E.L. Eskelinen, Autophagy: supporting cellular and organismal homeostasis by self-eating, Int. J. Biochem. Cell. Biol. 111 (2019) 1–10.

[22] S.K. Bhutia, S. Mukhopadhyay, N. Sinha, D.N. Das, P.K. Panda, S.K. Patra, T.K. Maiti, M. Mandal, P. Dent, X.Y. Wang, S.K. Das, D. Sarkar, P.B. Fisher, Autophagy: cancer's friend or foe? Adv. Cancer. Res. 118 (2013) 61–95.

[23] F. Cecconi, B. Levine, The role of autophagy in mammalian development: cell makeover rather than cell death, Dev. Cell 15 (2008) 344–357.

[24] Y.C. Kim, K.L. Guan, mTOR: a pharmacologic target for autophagy regulation, J. Clin. Invest. 125 (2015) 25–32.

[25] Q. Dou, H.N. Chen, K. Wang, K. Yuan, Y. Lei, K. Li, J. Lan, Y. Chen, Z. Huang, N. Xie, L. Zhang, R. Xiang, E.C. Nice, Y. Wei, C. Huang, Ivermectin induces cytostatic autophagy by blocking the PAK1/Akt axis in breast cancer, Cancer Res. 76 (2016) 4457–4469.

[26] D.W. Kang, B.H. Lee, Y.A. Suh, Y.S. Choi, S.J. Jang, Y.M. Kim, K.Y. Choi, D.S. Min, Phospholipase D1 inhibition linked to upregulation of ICAT blocks colorectal cancer growth hyperactivated by Wnt/beta-Catenin and PI3K/Akt Signaling, Clin. Cancer Res. 23 (2017) 7340–7350.

[27] B. Liu, S. Pan, Y. Xiao, Q. Liu, J. Xu, L. Jia, LINC01296/miR-26a/GALNT3 axis contributes to colorectal cancer progression by regulating O-glycosylated MUC1 via PI3K/AKT pathway, J. Exp. Clin. Cancer Res. 37 (2018) 316.

[28] R.E. Dorig, A. Marcil, A. Chopra, C.D. Richardson, The human CD46 molecule is a receptor for measles virus (Edmonston strain), Cell 75 (1993) 295–305.

[29] J.M. Gump, L. Staskiewicz, M.J. Morgan, A. Bamberg, D.W. Riches, A. Thorburn, Autophagy variation within a cell population determines cell fate through selective degradation of Fap-1, Nat. Cell Biol. 16 (2014) 47–54.

[30] E. Galanis, P.J. Atherton, M.J. Maurer, K.L. Knutson, S.C. Dowdy, W.A. Cliby, P. Haluska, Jr., H.J. Long, A. Oberg, I. Aderca, M.S. Block, J. Bakkum-Gamez, M.J. Federspiel, S.J. Russell, K.R. Kalli, G. Keeney, K.W. Peng, L.C. Hartmann, Oncolytic measles virus expressing the sodium iodide symporter to treat drug-resistant ovarian cancer, Cancer Res. 75 (2015) 22–30.

[31] E. Galanis, L.C. Hartmann, W.A. Cliby, H.J. Long, P.P. Peethambaram, B.A. Barrette, J.S. Kaur, P.J. Haluska, Jr., I. Aderca, P.J. Zollman, J.A. Sloan, G. Keeney, P.J. Atherton, K.C. Podratz, S.C. Dowdy, C.R. Stanhope, T.O. Wilson, M.J. Federspiel, K.W. Peng, S.J. Russell, Phase I trial of intraperitoneal administration of an oncolytic measles virus strain engineered to express carcinoembryonic antigen for recurrent ovarian cancer, Cancer Res. 70 (2010) 875–882.

[32] K. Garber, China approves world's first oncolytic virus therapy for cancer treatment, J. Natl. Cancer Inst. 98 (2006) 298–300.

[33] R.H. Andtbacka, H.L. Kaufman, F. Collichio, T. Amatruda, N. Senzer, J. Chesney, K.A. Delman, L.E. Spitler, I. Puzanov, S.S. Agarwala, M. Milhem, L. Cranmer, B. Curti, K. Lewis, M. Ross, T. Guthrie, G.P. Linette, G.A. Daniels, K. Harrington, M.R. Middleton, W.H. Miller, Jr., J.S. Zager, Y. Ye, B. Yao, A. Li, S. Doleman, A. VanderWalde, J. Gansert, R.S. Coffin, Talimogene laherparepvec improves durable response rate in patients with advanced melanoma, J. Clin. Oncol., 33 (2015) 2780-2788.

[34] S. Downs-Canner, Z.S. Guo, R. Ravindranathan, C.J. Breitbach, M.E. O'Malley, H.L. Jones, A. Moon, J.A. McCart, Y. Shuai, H.J. Zeh, D.L. Bartlett, Phase 1 Study of intravenous oncolytic poxvirus (vvDD) in patients with advanced solid cancers, Mol. Ther. 24 (2016) 1492–1501.

[35] N. Lalaoui, L.M. Lindqvist, J.J. Sandow, P.G. Ekert, The molecular relationships between apoptosis, autophagy and necroptosis, Semin. Cell Dev. Biol. 39 (2015) 63–69.

[36] I. Dikic, Z. Elazar, Mechanism and medical implications of mammalian autophagy, Nat. Rev. Mol. Cell. Biol. 19 (2018) 349–364.

[37] C.A. Lamb, T. Yoshimori, S.A. Tooze, The autophagosome: origins unknown, biogenesis complex, Nat. Rev. Mol. Cell. Biol. 14 (2013) 759–774.

[38] M.H. Sahani, E. Itakura, N. Mizushima, Expression of the autophagy substrate SQSTM1/p62 is restored during prolonged starvation depending on transcriptional upregulation and autophagy-derived amino acids, Autophagy 10 (2014) 431–441.

[39] M.C. Maiuri, E. Zalckvar, A. Kimchi, G. Kroemer, Self-eating and self-killing: crosstalk between autophagy and apoptosis, Nat. Rev. Mol. Cell. Biol. 8 (2007) 741–752.

[40] R. Amaravadi, A.C. Kimmelman, E. White, Recent insights into the function of autophagy in cancer, Genes Dev. 30 (2016) 1913–1930.

[41] S. Lal, D. Carrera, J.J. Phillips, W.A. Weiss, C. Raffel, An oncolytic measles virus-sensitive Group 3 medulloblastoma model in immune-competent mice, Neuro-oncol. 20 (2018) 1606–1615.

[42] G. Ungerechts, C. Springfeld, M.E. Frenzke, J. Lampe, W.B. Parker, E.J. Sorscher, R. Cattaneo, An immunocompetent murine model for oncolysis with an armed and targeted measles virus, Mol. Ther. 15 (2007) 1991–1997.

[43] H.T. Ong, M.J. Federspiel, C.M. Guo, L.L. Ooi, S.J. Russell, K.W. Peng, K.M. Hui, Systemically delivered measles virus-infected mesenchymal stem cells can evade host immunity to inhibit liver cancer growth, J. Hepatol. 59 (2013) 999–1006.

[44] E.K. Mader, G. Butler, S.C. Dowdy, A. Mariani, K.L. Knutson, M.J. Federspiel, S.J. Russell, E. Galanis, A.B. Dietz, K.W. Peng, Optimizing patient derived mesenchymal stem cells as virus carriers for a phase I clinical trial in ovarian cancer, J. Transl. Med. 11 (2013) 20.

[45] E.S. Bah, R.A. Nace, K.W. Peng, M. Muñoz-Alía, S.J. Russell, Retargeted and stealth–modified oncolytic measles viruses for systemic cancer therapy in measles immune patients, Mol. Cancer Ther. 19 (2020) 2057–2067.